# Towards Contactless, Low-Cost and Accurate 3D Fingerprint Identification

Ajay Kumar, Cyril Kwong

**Abstract**—Human recognition using fingerprint impressions has been widely studied and employed for more than 2000 years. Despite new advancements in 3D imaging technologies, widely accepted representation of 3D fingerprint features and matching methodology is yet to emerge. This paper investigates 3D representation of widely employed 2D minutiae features by recovering and incorporating (i) minutiae height z and (ii) its 3D orientation $\phi$ information and develops an effective matching strategy for matching popular minutiae features extended in 3D space. One of the obstacles of the emerging 3D fingerprint identification systems to replace the conventional 2D fingerprint system lies in their bulk and high cost, which is mainly contributed from the usage of structured lighting system or multiple cameras. This paper attempts to addresses such key limitations of the current 3D fingerprint technologies by developing the single-camera-based 3D fingerprint identification system. We develop a generalized 3D minutiae matching model and recover extended 3D fingerprint features from the reconstructed 3D fingerprints. 2D fingerprint images acquired for the 3D fingerprint reconstruction can themselves be employed for performance improvement and has been illustrated in the work described in this paper. This paper also attempts to answer one of the most fundamental questions on the availability of inherent discriminable information from 3D fingerprint. The experimental results are presented on a database of 240 client's 3D fingerprints, which is made publicly available to further research efforts in this area, and illustrate discriminant power of 3D minutiae representation and matching to achieve performance improvement.

**Index Terms** — Biometrics, Fingerprint Recognition, Personal Identification, Contactless and 3D Fingerprint Identification.

— — — — — — — — — ◆ — — — — — — — — —

## 1. INTRODUCTION

BIOMETRICS based human identification is one of the most critical and challenging tasks to meet the growing demand for stringent security. The fingerprints impressions have been used for personal identification for over 2000 years and automated fingerprint identification systems have been used for decades. Compared with other extrinsic biometric features, fingerprint is considered to be the most invariant and reliable, and occupies the largest share in the global biometrics market. Nearly all forensics and law enforcement agencies worldwide utilize Automatic Fingerprint Identification Systems (AFIS). Emergence of low-cost and compact fingerprint readers has made fingerprint modality a preferred choice in a wide range of civilian and commercial applications.

The *traditional acquisition of fingerprint scans* by pressing or rolling of the finger against the hard surface (glass, silicon, polymer) or paper often results in partial or degraded quality images due to improper finger placement, skin deformation, slippages, smearing or sensor noise. Live fingerprint scans employed for commercial and law-enforcement applications often have to cope with the residue of dirt, moisture, and sweat left from the previous fingerprint scans, *e.g.*, manual cleaning of the sensor surface. The non-contact, *i.e.*, contactless or touchless fingerprint systems can avoid direct contact between the imaging sensor and the elastic finger surface. Such contactless fingerprint imaging approach can avoid fingerprint deformation and achieve higher accuracy in the automated fingerprint recognition.

- Ajay Kumar and Cyril Kwong are with the Department of Computing, The Hong Kong Polytechnic University, Hong Kong;

**Table 1**: Touch-based Vs Contactless 2D/3D Fingerprint Identification.

| | Touch Based 2D Fingerprint | Contactless 2D Fingerprint | | Contactless 3D Fingerprint |
|---|---|---|---|---|
| *Recognition Accuracy* | High | High | √ | Very High |
| *Security/Hazards with Sensor Usage* | High | Very Low | √ | Very Low |
| *Skin Deformation* | High | NIL | √ | NIL |
| *Sensor Surface Smear/Noise* | High | Very Low | √ | Very Low |
| *Identification of Spoof and Alterations* | Low | Medium | √ | High |
| *Cost* | Low | High | × | Very High |
| *Bulk/Size* | Compact | Medium/Large | × | Bulky |

### 1.1 Motivation and Related Work

Automated fingerprint identification has been widely studied in last two decades and significant advancements have been made to deliver relatively good performance. However, the performance from the state-of-the-art fingerprint matchers is still much below [5], [28] the expectations and theoretical estimation. Increasing use of fingerprint identification technologies in a very large scale of applications, *e.g. Aadhaar* project [39] to identify billion plus people, and under wide-operating scenarios/conditions have further raised the expectations from fingerprint recognition technologies. Therefore further efforts are required to improve the accuracy, speed and convenience in the use/deployment of fingerprint recognition technologies. In order to avail the benefits of higher user convenience, hygiene, and improved accuracy, contactless 3D fingerprint recognition techniques (Table 1) have recently been introduced in the literature [1], [3]-[4], [33]. Parziale *et al.* [1], [8] have proposed a contactless fingerprint identification system that uses multiple cameras to systematically acquire multiple views of the presented finger. These views are combined to reconstruct 3D representation of the acquired fingerprint. The core technology in this system is based on the *shape from silhouette*, which requires views of fingerprint from different viewpoints and under different illuminations. The corresponding silhouettes are extracted to reconstruct 3D rep-

resentation of fingerprint images. While the *shape from silhouette* approach for the 3D fingerprint reconstruction can significantly reduce the fingerprint deformations, it has not been successful to exploit 3D fingerprint ridge details. In order to address such limitations, Wang *et al.* [3]-[4] have recently proposed the use of 3D fingerprint reconstruction under structured lighting illumination using phase measuring profilometry which can also record 3D ridge details. This is a highly exciting effort which has shown its promises on the database of 11 subjects with genuine accept rate of ~45% at 0.1% false acceptance rate when only relying on such 3D ridge matches. Both of these 3D fingerprint recognition systems [1], [3] have demonstrated to achieve higher recognition accuracy and response time than currently popular conventional 2D fingerprint technologies. There are several other promising references [40]-[41] which detail contactless 3D fingerprint identification techniques and the proposed fingerprint unwrapping models [37], [42] to match 3D fingerprint images with 2D fingerprint images which are largely available in legacy databases. One of the key limitations of these emerging 3D fingerprint technologies to replace the conventional 2D fingerprint system is their bulk and high cost, which mainly results from the nature of imaging technologies employed for the 3D fingerprint reconstruction. In [3] five cameras are required while the system in [1], [8] requires a specialized projector and a high-speed camera to implement 3D fingerprint scanning. Therefore there is a strong motivation and need to develop low-cost solutions for 3D fingerprint identification. It may be noted that [14], [38] the availability of low-cost 2D fingerprint imaging techniques is the key reason for the popularity of 2D fingerprint technologies that are widely deployed today. Therefore low-cost 3D fingerprint technologies can significantly enhance the applicability of such fingerprint recognition technologies in a wide range of civilian and commercial applications.

## 1.2 Our Work and Contributions

This paper focuses on addressing key limitations of current 3D fingerprint recognition technologies by developing 3D fingerprint minutiae representation and matching model that can account for the live 3D finger surface characteristics to recover extended fingerprint features, from *3D fingerprint images reconstructed from a single 2D imaging sensor*, and adaptively match them for accurate fingerprint identification. We recover the 3D profile of the fingerprint surface using a single camera, with a fixed viewpoint, that simultaneously acquires/uses multiple 2D fingerprint images under different illuminations. Such photometric-stereo inspired approach can provide a low-cost alternative to the currently available 3D fingerprint recognition systems which either use structured lighting [3], [31] or multiple cameras [35]. The accuracy of recovering surface normal using photometric stereo is higher than that possible by using triangulation based methods which is primarily due to the fact that such approaches estimate the depth of 3D surface and requires differentiation of depth map for computing/estimating surface normal. In addition to the lower cost and bulk resulting

from the use of single fixed camera, the developed approach can also help to enhance the anti-spoofing capabilities while significantly improving the accuracy of contactless 2D fingerprint recognition as the extended fingerprint features are simultaneously integrated for the performance improvement. The experimental result show that the developed standalone single camera-based contactless 3D fingerprint system can achieve significantly improved performance, than using only contactless 2D fingerprint images, both for verification and recognition applications.

The key contributions of this paper can be summarized as follows:

1. Among the variety of popular features, *e.g.*, minutiae, ridge feature map, orientation field, *etc.*, available for the fingerprint recognition, minutiae features are considered as most reliable [5], [28] and also widely employed by the law-enforcement experts and most of the commercial fingerprint systems available today. Their location in X-Y plane, type, and orientation is considered to be the most distinctive for the conventional fingerprint recognition. This paper attempts to further improve such distinctiveness by incorporating (i) minutiae height $z$ and (ii) its 3D orientation $\phi$. We systematically develop and evaluate composite matching strategy for the resulting 3D minutiae[1] representation using experimental results from the real 3D fingerprint dataset.

2. A new framework for *3D fingerprint identification* using *single fixed camera* is proposed. We reconstruct 3D fingerprint images using such imaging to identify and recover 3D minutiae fingerprint features and present *comparative performance* from the matching of reconstructed 3D fingerprint surface by using the local curvature information. The 2D fingerprint images acquired for the 3D fingerprint image reconstruction can themselves be also employed to further improve the matching accuracy for 3D fingerprint identification. We illustrate such experimental results from a 240 client's 3D fingerprint database which suggest the success of the single-camera-based approach for the contactless 3D fingerprint identification.

3. We attempt to answer one of the most fundamental questions on the availability of inherent discriminable information from the 3D fingerprints (further details in section 4.5). This paper also develops a unified matic (section 4.3) to match such 3D minutiae features which can account for *nonlinear* variations in the 3D fingerprint features, and achieve superior performance than the linear strategy.

4. Lack of any 3D fingerprint database in public domain is one of the limitations to promote further research efforts in this area. Therefore we also introduces first 3D fingerprint database in public domain consisting of 100,80 fingerprint images acquired from 240 clients.

Rest of this paper is organized as follows. In section 2, the system is overviewed with the help of a simplified block-

---

[1] This approach of 3D minutiae representation and matching is *generalized* with wide applications, and can also be employed to match 3D fingerprint images reconstructed from structured lighting imaging or using multiple cameras.
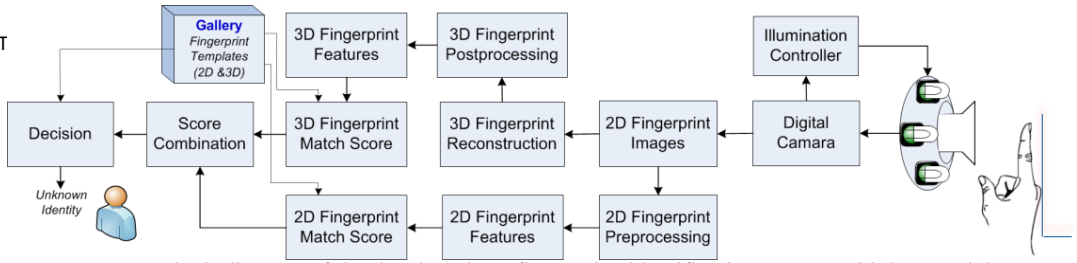
**Figure 1:** Block diagram of the developed 3D fingerprint identification system with key modules.

diagram of the developed system. Section 3 presents the methodology for 3D fingerprint reconstruction employed in this work. This section also details the postprocessing performed on the reconstructed 3D fingerprints. The feature extraction and matching strategy developed in this paper is detailed in section 4 while section 5 details the surface curvature based approach for the 3D fingerprint matching. The experimental results are illustrated in section 6. Section 7 presents' the summary of key conclusions from this paper and suggests further work directions.

## 2. SYSTEM OVERVIEW AND BLOCK DIAGRAM

A simplified block diagram of the single-camera based 3D fingerprint identification approach developed in this paper is illustrated in figure 1. This work uses a calibrated setup of multiple light (LED) sources in space which illuminate in a sequence to acquire multiple 2D fingerprint images. We also developed the required hardware to control the illumination sequence and synchronize the image acquisition using a computer (with the help of a graphical user/imaging interface which ia developed for this system, please see supplementary material). We employ seven symmetrically distributed LED for the illumination and a low-cost digital camera which can acquire 1280 × 1024 pixel images with 15 frames per second. We make several assumptions which are quite standard for photometric stereo based 3D image reconstruction; single point source is used to illuminate the fingerprint surface at infinity, the camera is orthographic and all its parameters are known. The position of LEDs on the acquired images is calibrated and the fingerprint surface is assumed to be described by Lambertian surface with constant albedo.

## 3. 3D FINGERPRINT RECONSTRUCTION USING PHOTOMETRIC STEREO

The reconstruction of fingerprint is based on the shape from shading technique. Given a 2D image $E(x, y)$, the shape from shading technique is used in this work to recover 3D fingerprint surface $z(x, y)$. The surface reflectance $R$ relates the observed 2D fingerprint image pixel intensities in $E(x, y)$ to the surface orientations/gradients for a given source direction and the surface reflectance in the direction of imaging/camera as in the following.

$$E(x, y) = \rho I_0 R(p(x, y), q(x, y)) \tag{1}$$

where $\rho$ is the albedo and $I_0$ is the incident radiance. The surface gradients $p(x, y)$ and $q(x, y)$ can be defined as follows:

$$p(x, y) = \partial f(x, y)/\partial x, q(x, y) = (\partial f(x, y))/\partial y \tag{2}$$

The 3D fingerprint surface can be reconstructed by recovering the surface height information $z = f(x, y)$. We approximate/consider finger surface as the Lambertian surface which is illuminated by multiple, say $m$, fixed light sources, i.e., $\mathbf{L} = [l^1, l^2, ... l^m]^T$. Each of these light sources (LED's) is fixed with a known direction $l = [l_x, l_y, l_z]^T$ and

radiance$\|l\|$. Let $\mathbf{n} = [n_x, n_y, n_z]^T$ be the unit surface normal vectors at some point of interest on the 3D fingerprint surface. The observed image pixel intensities $\mathbf{y}$, from the $m$ 2D fingerprint images, corresponding to the respective illumination sources can be written as follows;

$$\mathbf{y} = \mathbf{L} \cdot \mathbf{x} \tag{3}$$

where $\mathbf{y} = [y_1, y_2, ... y_m]^T$ and $\mathbf{x} = \rho[n_x, n_y, n_z]^T$. We assume that the light source directions are not co-planer so that the matrix $\mathbf{L}$ is non-singular. Equation (3) illustrates a linear relationship between 3D fingerprint surface, observed pixel intensities from 2D fingerprint image and the unit surface normal vectors $\mathbf{x}$. The unknown vector $\mathbf{x}$ can be estimated from the standard [2], [6] least squared error technique using the following equation.

$$\mathbf{x} = (\mathbf{L}^T \mathbf{L})^{-1} \mathbf{L}^T \mathbf{y} \equiv \rho \mathbf{n} \tag{4}$$

Since $\mathbf{n}$ is of unit length, the length of recovered vector $\mathbf{x}$ is the absolute reflectance (albedo) $\rho$ and the surface normal is represented by the direction of unit vector $\mathbf{n}$. The recovered surface normals are then integrated to recover the 3D fingerprint surface $z(x, y)$.

### 3.1 Postprocessing Reconstructed 3D Fingerprints

The reconstructed 3D fingerprint is essentially 3D cloud point data which requires some processing to suppress the accompanying noise. This cloud point data $z(x, y)$ is firstly subjected to smoothing process which firstly applies a 5 × 5 median filter to suppress speckle-like noise. The resulting image is then subjected to 3D variant of Laplacian smoothing which has been found to be quite effective in denoising point clouds [9], [20]. For a vertex $z_i$ within the image $z = f(x, y)$, with its neighbors $z_j$, the updated vertexes $\bar{z}_i$ are computed as follows:

$$\bar{z}_i = (1 - \epsilon)z_i + \frac{\epsilon}{\sum_j w_{ij}} \sum_j w_{ij} z_j \tag{5}$$

where $w_{ij}$ is a finite support weighting function and is chosen as the inverse of distance between vertex $z_i$ and its neighbors $z_j$, i.e., $w_{ij} = \|z_j - z_i\|^{-1}$. The reconstructed 3D fingerprint surface is smoothed after 40 iterations with $\epsilon = 0.5$ and the neighbors $j$ are chosen within ±2 pixel in the $x$ and $y$ directions from vertex $z_i$

The normal vectors of the cloud point fingerprint data for the smoothed surface are then computed by the gradient of $z = f(x, y)$. The normal vector is an upward normal with ($-g_x$, $-g_y$, 1), where $g_x$ and $g_y$ are the gradient along $x$ and $y$ directions. These normalized surface normals are then used for estimating the principle curvature as will be detailed in section 5.

## 4. FEATURE EXTRACTION AND MATCHING

The 3D representation of minutiae and corresponding matching strategy is introduced in this section (4.2). During 3D fingerprint reconstruction, we ignore those pixels in the acquired 2D fingerprint images which can be considered as being influenced by specular reflection. One of

the simpler but effective approaches is to consider top $k$% high intensity pixels from all the 2D fingerprint images, with different illumination profile which are acquired for a 3D fingerprint reconstruction, as the specular reflections. The magnitude of $k$ is empirically determined and set as 0.228.

Each of the 2D fingerprint images acquired for the 3D fingerprint reconstruction, although with varying illumination profile, can also be simultaneously exploited for the 2D minutiae extraction and matching[2], which is briefly summarized in the following section. Since *2D fingerprint images* are acquired from *a distance* (figure 1), which is ~10 cm during our imaging, the observed contrast of intensity between the valley and the ridge is quite low. Therefore each of the acquired images requires contrast enhancement before subjecting them to Gabor filter based [5], [15] fingerprint enhancement algorithm. In this work we use homomorphic filters based contrast enhancement approach which has been described in reference [1].

## 4.1 *Conventional* Minutiae Representation in 2D Space and Matching

Each of the enhanced 2D fingerprint images are used to locate the minutiae features using the conventional approach [21]. We select a minutiae pair, consisting of a minutia from the reference template image ($Q$) and a minutia from the query template image ($P$), to generate match distances between them using the alignment-based approach. All the other minutiae in $P$ are also converted to the spherical coordinate as $[r, A_s, A_\theta, T]$ which center at the reference minutia in $Q$ and align the angle with $\theta_{ref}$.

$$r = \sqrt{(x - x_r)^2 + (y - y_r)^2} \tag{5}$$

$$A_s = \text{atan2}\left(\frac{y - y_r}{x - x_r}\right) - \theta_r \tag{6}$$

$$A_\theta = (\theta - \theta_r) \tag{7}$$

where $r$ is the distance of respective minutiae with the reference minutia, $A_s$ is the angular separation of the minutia, $A_\theta$ is the orientation of the minutia, and $T$ is the type of minutia. If the difference between $[r_i, A_{si}, A_{\theta i}, T_i]$ in $P$ and $[r_j, A_{sj}, A_{\theta j}, T_j]$ in $Q$ is smaller than a predetermined threshold and $T_i = T_j$, then the minutia $i$ in $P$ and minutia $j$ in $Q$ are considered as the matched pair. The matching score is generated by the popular approach as follows:

$$S_{2D} = \frac{m^2}{M_P M_Q} \tag{8}$$

where $m$ is the total number of matched minutiae pairs and $M_P$, $M_Q$ is the number of minutiae in query and template image respectively. The maximum score of all the possible reference minutia pair in $P$ is selected as the final matching score between fingerprint image $P$ and $Q$.

## 4.2 *Extended* Minutiae Representation in 3D Space and Matching

Conventional fingerprint templates typically include 2D minutiae details ($x$, $y$, $\theta$, $q$) consisting of position of the minutiae ($x$, $y$) along with the angle $\theta$ representing the

orientation of the minutiae and the quality $q$ of minutiae [24]. We can extend such 2D minutiae templates to include 3D details by adding two features $z$ and $\phi$. The value $z$ is the height of the vertex on the reconstructed 3D fingerprint surface at position ($x$, $y$) while $\theta$ and $\phi$ represent the minutiae orientation in spherical coordinates with unit length 1. The angle $\phi$ can be computed by tracing (figure 3) the reconstructed 3D fingerprint surface at
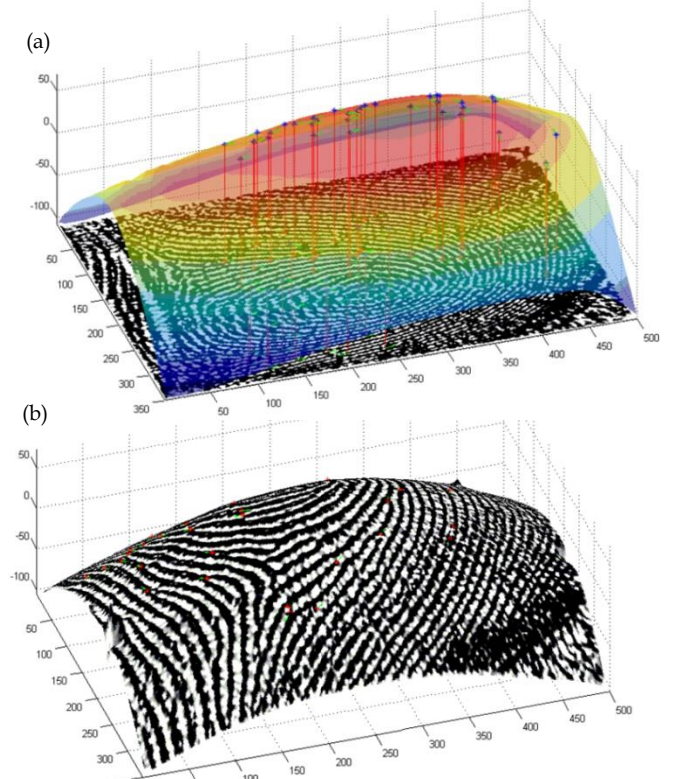


**Figure 2**: Reconstructed 3D fingerprint image illustrating (a) extended minutiae feature information in 3D space and (b) surface curvature from a typical fingerprint image.
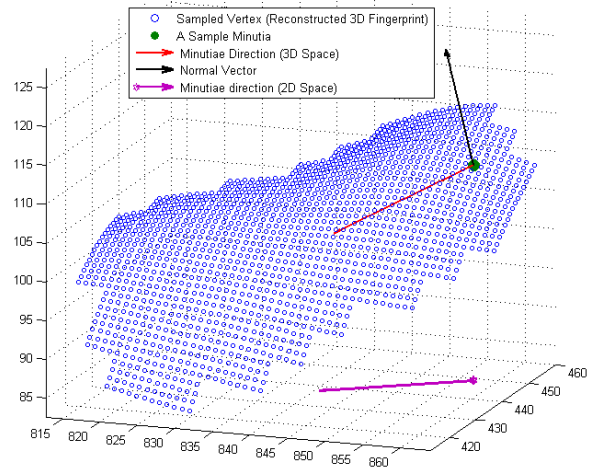


**Figure 3**: Using 2D minutia direction (purple arrow) defines local ridge surface (blue dot) to estimate 3D minutia direction (red arrow).

minutiae locations along the direction of $\theta$, which is available from 2D minutiae details ($x$, $y$, $\theta$). In case of bifurcation type of minutiae, the local ridge surface is utilized (or masked) while local valley surface is masked for the end type of minutiae since the direction $\theta$ is here pointing in

---

an outward direction. The angle $\phi$ is then computed by estimating the principle axes [16] of the masked ridge surface. The extended minutiae representation in 3D space can be localized as $(x, y, z, \theta, \phi)$, where $(x, y, \theta)$ is the respective minutiae representation in 2D space. In rest of this paper, the extended minutiae representation $(x, y, z, \theta, \phi)$, is referred to as 3D minutiae.

## 4.3 Matching Extended Minutiae Representation in 3D Space

The 3D minutia matching algorithm developed to generate the matching score between two 3D minutiae from the two fingerprint templates, say $P$ and $Q$, is detailed in the following. Firstly a reference minutia from the template $P$ and template $Q$ are selected and all the other minutiae are transformed to the spherical coordinates. Then the (two) reference minutiae are aligned with the $x$-axes and $z$-axes. This alignment ensures that the aligned reference minutiae (in both template $P$ and $Q$) location can serve as the universal origin/reference (figure 4) to measure other minutiae distances in the respective templates. If an aligned minutia is represented as $m_r = [x_r, y_r, z_r, \theta_r, \phi_r]$ in template $P$, the relative representation of other 3D minutiae in template $P^3$, say $m$ (see figure 4 to visualize relative representation of two 3D minutiae), can be denoted as $m = [r, A_s, A_\theta, A_g, A_\phi]$; where $r$ is the radial distance with reference minutiae, $A_\theta$ is the azimuth angle and $A_\phi$ is the elevation angle that localizes the minutiae $m$ in 3D plane, while $A_s$ and $A_g$ are the azimuth and the elevation angles respectively that localize the radial vector $r$ (with respect to reference minutiae $m_r$) in 3D space. Let $R_z(\theta)$ and $R_y(\phi)$ be the rotation matrix along $z$ and $y$ direction in cartesian coordinate, and sph$(x, y, z)$ be the cartesian to spherical coordinate transformation with unit length 1:

$$R_z(\theta) = \begin{bmatrix} \cos\theta & -\sin\theta & 0 \\ \sin\theta & \cos\theta & 0 \\ 0 & 0 & 1 \end{bmatrix}, \ R_y(\phi) = \begin{bmatrix} \cos\phi & 0 & -\sin\phi \\ 0 & 1 & 0 \\ \sin\phi & 0 & \cos\phi \end{bmatrix}$$

$$\text{sph}([x \ y \ z]) = [\text{atan2}(y,x) \ \sin^{-1}z] \quad (9)$$

where atan2 is the four-quadrant inverse tangent function [25]. The parameters for the relative representation (feature vector) of minutiae $m$ are computed as follows:

$$r = \sqrt{(x - x_r)^2 + (y - y_r)^2 + (z - z_r)^2} \quad (11)$$

$$[x'y'z']^T = R_y(-\phi_r)R_z(-\theta_r)\frac{1}{r}[x - x_r \ y - y_r \ z - z_r]^T \quad (12)$$

$$[A_s \ A_g] = \text{sph}([x'y'z']) \quad (13)$$

$$[A_\theta \ A_\phi] = \text{sph}\left(\left(R_y(-\phi_r)R_z(-\theta_r)(\text{sph}^{-1}([\theta \ \phi]))^T\right)^T\right) \quad (14)$$

Two 3D minutiae in the two fingerprint template $P$ and $Q$ are considered as the matched pair if the difference between their feature vectors $(r_{Pi}, A_{s_{Pi}}, A_{\theta_{Pi}}, A_{g_{Pi}}, A_{\phi_{Pi}})$ and $(r_{Qi}, A_{s_{Qi}}, A_{\theta_{Qi}}, A_{g_{Qi}}, A_{\phi_{Qi}})$ is smaller than a given threshold (or tolerance limit).

$$\Delta r = |r_{Pi} - r_{Qj}| \quad (15)$$

$$\Delta_{A_s} = \min\left(\left|A_{s_{Pi}} - A_{s_{Qj}}\right|, 360° - \left|A_{s_{Pi}} - A_{s_{Qj}}\right|\right) \quad (16)$$

$$\Delta_{A_\theta} = \min\left(\left|A_{\theta_{Pi}} - A_{\theta_{Qj}}\right|, 360° - \left|A_{\theta_{Pi}} - A_{\theta_{Qj}}\right|\right) \quad (17)$$

$$\Delta_{A_g} = \left|A_{g_{Pi}} - A_{g_{Qj}}\right| \quad (18)$$

$$\Delta_{A_\phi} = \left|A_{\phi_{Pi}} - A_{\phi_{Qj}}\right| \quad (19)$$

If $\Delta r \le th_r$, $\Delta_{A_s} \le th_{A_s}$, $\Delta_{A_\theta} \le th_{A_\theta}$, $\Delta_{A_g} \le th_{A_g}$, and $\Delta_{A_\phi} \le th_{A_\phi}$, the minutiae pair from $P$ and $Q$ is considered as matched. Total numbers of such matched minutiae pairs (figure 5) are computed. The *maximum* number of matched minutiae pairs, among all the possibilities of every minutiae in $P$ and $Q$ being used as a reference, is used to compute the matching score. This matching score between the two 3D minutia templates $P$ and $Q$ is computed as follows:

$$S_{3D} = \frac{m^2}{M_P M_Q} \quad (20)$$

where $m$ is the total number of matched minutiae pairs and $M_P$, $M_Q$ is the number of minutiae in template $P$ and $Q$ respectively.
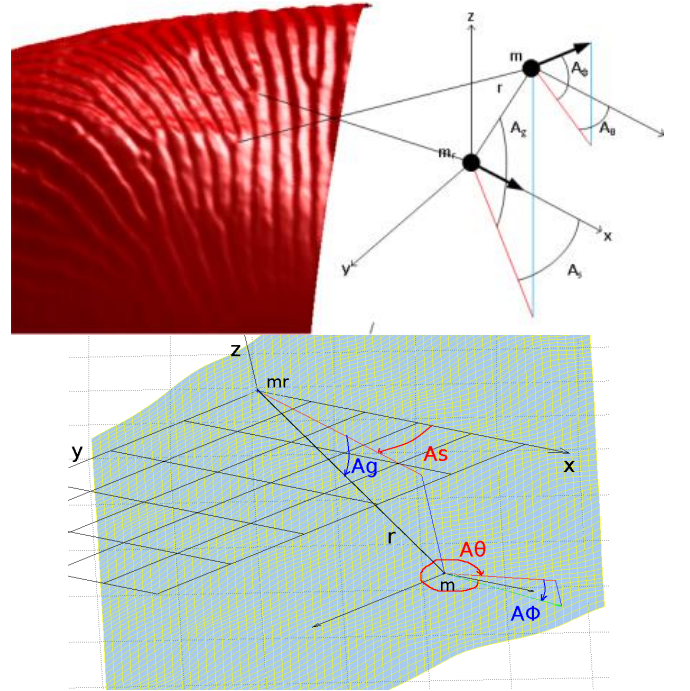


**Figure 4**: Relative localization of a 3D minutiae with a reference minutiae $(m_r)$ in a given 3D fingerprint template using relative distances/angles between the reference 3D minutia $(m_r)$ and other 3D minutia $(m)$. The $x$ axis of cartesian coordinate is aligned with the direction of $m_r$ (the bold arrow). The azimuthal angles $A_s$ and $A_\theta$ are in the range of [0, 360] degree. The polar angles $A_g$ and $A_\phi$ are in the range of [-90, 90] degree. It may be noted that the magnitude/value of $(r, A_s, A_\theta, A_g, A_\phi)$ are *exaggerated* simply to illustrate these values clearly (rather than use exact from upper left hand side image) and most of the finger surface is convex. In the lower figure, the green line for m illustrates orientation of 3D minutiae while the red line illustrates its projection in x-y plane.

The fingerprint matching can be more effective [45] with the use of a function to compute the similarity score of minutiae and a threshold for the rejection of falsely matched minutiae. Assuming that there are some falsely matched minutiae pairs after the hard threshold, it is possible to reject some of them by transforming all features to a scalar product. Therefore we explored a unified matching distance function for matching two 3D minutiae which can reject falsely matched minutiae using comparison with a fixed decision threshold (calibrated during training stage). This function to combine the difference
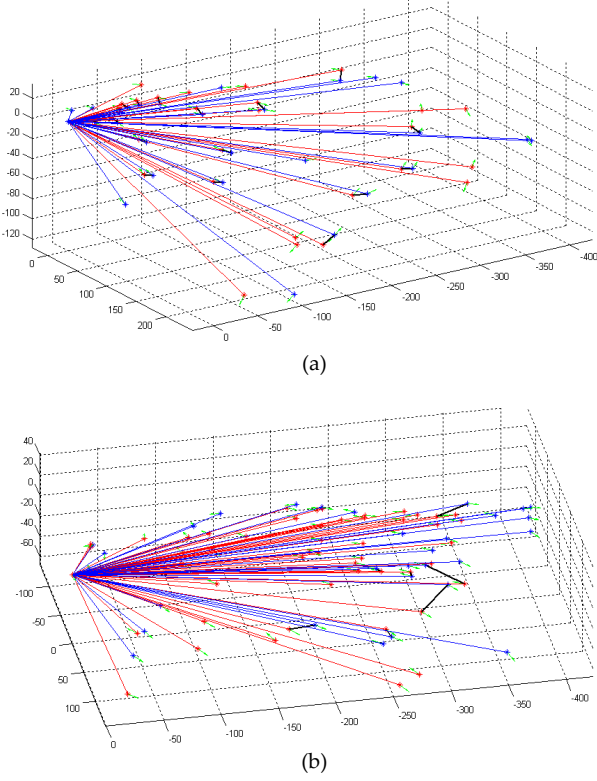
---

[3] Also in template $Q$ since the reference minutiae have been aligned to serve as the universal reference/origin.

(a)



(b)

**Figure 5**: Matching two genuine 3D minutia templates in (a) and the imposter templates in (b) from template $P$ (in red color) and template $Q$ (in blue color). The color lines are links from the reference minutia while the black lines illustrate the minutiae pairs that are regarded as matched.

vector in (15)-(19) for generating a unified matching distance can be written as follows:

$$funRSG(\Delta v) = \left(\frac{\Delta r}{65}\right)^{0.8} + \left(\frac{\Delta A_s}{30}\right)^{0.8} + \left(\frac{\Delta A_g}{15}\right)^{0.8} + \left(\frac{\Delta A_\theta}{18}\right)^{0.8} + \left(\frac{\Delta A_\phi}{42}\right)^{0.8} + \left(\frac{1-cosN}{0.075}\right)^{0.8} (21)$$

where $\Delta v$ is the vector of difference values as computed in (14) and  $cosN$ is the value of normal vector (figure 3) cosine similarity between two matched minutiae. In our experiments (section 7), if $funRSG(\Delta v)$ is smaller than 1.825, then this pair of minutia is considered as the matched pair. The power term 0.8 makes the boundary of the high dimension space convex. Our study on the difference of such vectors (figure C in *supplementary file*) suggests that the equation (21) may be generalized to more accurately account for relative variations in feature distances as follows:

$$funRSG(\Delta v) = \left(\frac{\Delta r}{f(r)}\right)^{a} + \left(\frac{\Delta A_s}{A}\right)^{b} + \left(\frac{\Delta A_g}{B}\right)^{c} + \left(\frac{\Delta A_\theta}{C}\right)^{d} + \left(\frac{\Delta A_\phi}{f(r)}\right)^{e} + \left(\frac{1-cosN}{D}\right)^{f} (22)$$

which has an independent set of power term $\{a, b,...,f\}$ while $f(r)$ can be some function of distance. The matching score between two 3D minutiae template $P$ and $Q$ can be computed from equation (20) using the number of matched minutia pairs.

## 4.4  2D Minutiae Selection

The limiting accuracy of preprocessing and 3D reconstruction algorithm, finger movement and sensor/surface noise, often influences the accuracy and reliability of reconstructed 3D minutiae. Therefore recovered 3D minutiae which can be considered to have higher reliability are only utilized to achieve higher confidence in the matching process/results. If a 2D minutia from a spatial region is detected in more than one image, among the multiple 2D

fingerprint images acquired with different LED illuminations for the respective 3D fingerprint reconstruction, then its *corresponding* 3D minutiae from this region can be considered as more reliable. Such an algorithm (S3DM, figure 6) employed to automatically select 3D minutiae with higher reliability is discussed in the following.

Let the list of minutiae extracted from the 2D fingerprint image under the first LED illumination be $L = \{m_1, m_2, ... m_n\}$, where $m = [x, y, \theta, q]$. We firstly initialize the *counted list* $CL = \{cm_1, cm_2, ... cm_n\}$, where $cm = [x, y, \theta, q, c]$, $c$ is the  number of occurrence and is set to 1. For each minutia $m_i$ from the fingerprint  image under the second to the seventh LED illumination, the $CL$ is updated as follows: Let $\{TL\}$ is a subset of $CL$ such that $\|x_{cm,k} - x_i, y_{cm,k} - y_i\|^2 \leq$ k1 and $\min(|\theta_{cm,k} - \theta_i|, 360 - |\theta_{cm,k} - \theta_i|) \leq$ k2 where $cm_k \in CL$, then we update the $cm_t$ such that $c_t \geq c_i$ for all $cm_i \in \{TL\}$. $x, y, \theta, q$  value of updated $cm_t$ will be the average value of existing cluster members and new member, and $c$ will be increased by one. We choose k1 as 4 since the minutiae location in different (LED) fingerprint images would not shift too far away and square root of 4 (= 2) which is slightly smaller the half width of the observed ridge (~5 pixel in the employed fingerprint images). The constant k2 is set to 25 for the acceptable angle difference which can help to ensure that the clusters have similar direction while k3 is set to 32 to decrease the overlapping/double cluster with the similar direction and location. After updating $CL$, we pick

**Algorithm**: S3DM

```
Input: List of minutiae from 7 LED images {L₁,...,L₇}, where Lᵢ={m₁, m₂,... mₙ} and mₖ = [xₖ, yₖ ,ϑₖ, qₖ]
CL := {}  // the tuple of CL is [x, y, ϑ, q, c] where c is number of count
for each minutia mₖ in L₁ do
        CL := CL ∪ [xₖ, yₖ ,ϑₖ, qₖ, 1]
end for
for each minutia mₖ in L₂,L₃,...,L₇ do
        TL := {}
        for mᴄₗ ∈ CL do
                if‖x_CL − xₖ, y_CL − yₖ‖² ≤ k1 and min(|θ_CL − θᵢ|, 360 − |θ_CL − θₖ|) ≤ k2
                        TL := TL ∪ mᴄₗ
                end if
        end for
        if TL ≠ {}
                maxC := 0
                for mₜₗ ∈ TL do
                        if cₜₗ > maxC
                                mₜ := mₜₗ
                                maxC = cₜₗ
                        end if
                end for
                [xₜ,yₜ, θₜ, qₜ] := (cₜ*[xₜ,yₜ, θₜ, qₜ] + [xₖ, yₖ ,ϑₖ, qₖ])/(cₜ+1)
                mₜ := [xₜ,yₜ, θₜ, qₜ, cₜ+1]
        else
                CL = CL ∪ [xₖ, yₖ ,ϑₖ, qₖ, 1]
        end if
end for
DL := {}
for mᴄₗ ∈ CL do
        if cᴄₗ >= 2
                DL := DL ∪ mᴄₗ
        end if
end for
for m_DL ∈ DL do
        for mₖ ∈ DL do
                if if‖x_DL − xₖ, y_DL − yₖ‖² ≤ k3 and min(|θ_DL − θᵢ|, 360 − |θ_DL − θₖ|) ≤ k2
                        [xₖ, yₖ, ϑₖ, qₖ] := (c_DL*[x_DL, y_DL, ϑ_DL, q_DL] + cₖ* [xₖ, yₖ ,ϑₖ, qₖ])/(c_DL + cₖ)
                        m_DL := [xₖ, yₖ, ϑₖ, qₖ, c_DL + cₖ]
                        mₖ := {}
                end if
        end for
end for
Output: DL
```
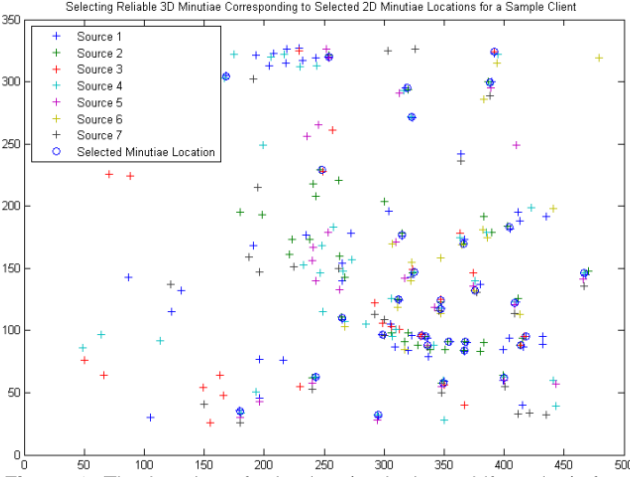
**Figure 6**: The location of minutiae (endpoint or bifurcation), from a sample clients 2D fingerprint images under different illuminations, with lighting (cross) and the clustered location (circle).

the subset of *CL* as *DL* with $c \geq 2$. If two cluster groups are too close, we merge them together to reduce the possibility that a single minutia is recovered as two minutiae. The final   list of   minutiae  is  the merged list of DL which is assumed (as shown from the experiments) to have higher reliability and matching. The 3D minutiae corresponding to these 2D minutiae locations are employed during matching stage. This strategy to select reliable 3D minutiae is summarized by the algorithm S3DM.

## 4.5 Improvement in Fingerprint Individuality using 3D Minutiae Matching

The recovery and matching of 3D minutiae is expected to significantly improve the (theoretical) estimates on the individuality of fingerprints. Such an upper limit on the performance of 3D fingerprint identification can be established from the theoretical estimates on the probability of false correspondence between two 3D minutiae based representations from arbitrary 3D fingerprints belonging to two different persons. Since fingerprint is the most popular and widely employed biometric modality today, our objective here is to theoretically ascertain such amount of improvement, over the conventional 2D fingerprint matching, which could also help to justify the higher complexity in the acquisition and matching of 3D fingerprints.

Let *V* be the overlapping volume between two arbitrary 3D fingerprint surface being matched while $H(p)$ be the height of the aligned surface with point *p* on the projection on X-Y plane. *V* can be estimated as follows:

$$U = \sum_{s=1}^{N} \sum_{t=1, t \neq s}^{N} \frac{\sum_{p \in A} |H(p)_s - H(p)_t|}{A(s,t)} \qquad (23)$$

$$\sigma = \sum_{s=1}^{N} \sum_{t=1, t \neq s}^{N} \frac{\left(\sum_{p \in A} (|H(p)_s - H(p)_t| - U)^2\right)}{A(s,t)} \qquad (24)$$

$$V = \left(U + 2\sqrt{\sigma}\right) A(s,t) \qquad (25)$$

where A(*s, t*) is the overlapped area on X-Y plane of two aligned surfaces *s* and *t*. The variance σ can be estimated by statistics of the reconstructed 3D fingerprint surface in the database and represents twice standard deviation limits that cover 95% confidence interval. The probability of matching *r* minutiae in two 3D fingerprint images or templates in spatial-location (*x, y, z*), direction *θ*, and di-

$$P_{3D}(J, m, n, r) = \sum_{p=r}^{\min(m,n)} \sum_{q=r}^{p} \left( \frac{\binom{m}{p}\binom{J-m}{n-p}}{\binom{J}{n}} \times \binom{p}{q} (l)^q (1-l)^{p-q} \times \binom{q}{r}(k)^r(1-k)^{q-r} \right) (26)$$

where *m* and *n* denote number of 3D minutiae in two 3D fingerprints being matched, *J* represents the nearest integer corresponding to $J = V/(\frac{4}{3}\pi r_0^3)$, and $r_0 = \Delta r$ (equation 15), while *l* and *k* respectively denote the probability of matching a 3D minutiae along orientation *θ* and along orientation *ϕ* once they are falsely matched at 3D location (*x, y, z*). Above estimation of false correspondence assumes that the angle *ϕ* and angle *θ* are independent of their location (*x, y, z*). Equation (26) is an extension of individuality model developed in [28] for 2D fingerprints and its derivation appears in appendix A. The probability of false random correspondence using conventional minutiae representation in 2D space *i.e.*, matching *q* minutiae both in spatial-location (*x, y*) and also along the direction *θ*, is given by [28]:

$$P_{2D}(M, m, n, q) = \sum_{p=q}^{\min(m,n)} \left( \frac{\binom{m}{p}\binom{M-m}{n-p}}{\binom{M}{n}} \times \binom{p}{q} (l)^q (1-l)^{p-q} \right) \qquad (27)$$

where *M* represents the nearest integer for $M = A/(\pi r_0^2)$. Assuming that the *same* two fingerprints are matched in 2D space and 3D space, and *J = M*, using (27) we can rewrite (26) as

$$P_{3D}(M, m, n, r) = \sum_{q=r}^{p} \left( \binom{q}{r}(k)^r(1-k)^{q-r} \right) \times P_{2D}(M, m, n, q) (28)$$

Above equation suggests that the probability of false random correspondence using the 3D minutiae matching is expected to be smaller, as compared to the case when only *respective* 2D minutiae matching is employed. The extent of such reduction depends on *k* [0-1], *i.e.*, nonlinearly decreases with the reduction in tolerance while matching angle *ϕ*. In practice *J > M* (which would further reduce the probability of false correspondence) and this assumption is only to compute upper bond of probability of false correspondence for the comparison. Our experiments (in section 7) also provide a typical example of improvement in the fingerprint individuality when the minutiae features are recovered and matched in 3D space.

## 5. ESTIMATING 3D FINGERPRINT SURFACE CURVATURE

The differential geometric properties of 3D surface are invariant under rigid transformation and can be potentially used to compute intrinsic 3D *fingerprint surface* descriptors to match two reconstructed 3D fingerprint surfaces. In this paper, we have also performed such study to exploit local differential geometric properties, *i.e.*, principal curvature, unit normal vector and surface directions, to ascertain their effectiveness for the fingerprint surface matching. The principal surface curvature typically measures *local* bending of fingerprint surface at each of the surface points while the principal surface directions indicate the directions of minimum and maximum surface bending. Several algorithms have been proposed in the literature to estimate the surface curvature using *local* surface fitting. Goldfeather and Interrante [10] have described three approaches, *i.e.*, quadratic surface approximation, normal surface approximation and adjacent-normal cubic order surface approximation. Among

these three approaches, adjacent-normal cubic order approximation algorithm works the best [2] and is used in our work.

Let a given surface point be $s$ with its normal $N$ and its $u$ neighbouring points be $t_i$ with their normal vectors $K_i$ where $i = 1, 2, \ldots u$. In the coordinate system with $s$ as the origin $(0, 0, 0)$ and $N$ as the $z$-axis, the position of neighbours $t_i$ is $(x_i, y_i, z_i)$ and the position of $K_i$ is $(a_i, b_i, c_i)$. Using the adjacent-normal cubic order algorithm, we essentially attempt to locate a surface that can fit the vertex and its neighbouring points such that:

$$z = f(x, y) = \frac{a}{2}x^2 + bxy + \frac{c}{2}y^2 + dx^3 + ex^2y + fxy^2 + gy^3 \tag{29}$$

The normal vector of the surface point $s$ in the approximated surface is written as

$$N(x, y) = \left(f_x(x, y), f_y(x, y), -1\right) \tag{30}$$
$$= (ax + by + 3dx^2 + exy + fy^2, bx + cy + ex^2 + 2fxy + 3gy^2, -1) \tag{31}$$

The cubic-order surface fitting, for both the neighboring surface points and their normal, generate following three

$$\begin{pmatrix} \frac{1}{2}x_i^2 & x_iy_i & \frac{1}{2}y_i^2 & x_i^3 & x_i^2y_i & x_iy_i^2 & y_i^3 \\ x_i & y_i & 0 & 3x_i^2 & 2x_iy_I & y_i^2 & 0 \\ 0 & x_i & y_i & 0 & x_i^2 & 2x_iy_i & 3y_i^2 \end{pmatrix} \Omega = \begin{pmatrix} z_i \\ -\frac{a_i}{c_i} \\ -\frac{b_i}{c_I} \end{pmatrix} \tag{32}$$

where $\Omega = [a\ b\ c\ d\ e\ f\ g]^T$ is the coefficient vector of the cubic surface. Above equation is an over determined equation system and can be written in the following form:

$$K\Omega = R \tag{33}$$

where $K$ is $3u \times 7$ matrix (from left hand side of equation 30) and R is $3u \times 1$ vector. We can apply least-square fit to find the best solution for equation (33) and construct Weingarten curvature matrix $W$ for the fitted surface using only three coefficients.

$$W = \begin{pmatrix} a & b \\ b & c \end{pmatrix} \tag{34}$$

The eiganvalues of Weigarten matrix are the maximum and minimum principle curvatures of the surface ($k_{max}$ and $k_{min}$), and their eigenvectors are the principal direction vectors ($h_{max}$ and $h_{min}$) which can be directly computed. The shape index of a surface at vertex $s$ can quantify the local 3D shape of the fingerprint surface. The curvature information described using shape index $C_i(s)$ is independent of scale and can be computed as follows [12]:

$$C_i(s) = \frac{1}{2} - \left(\frac{1}{\pi}\right) atan \left(\frac{k_{max} + k_{min}}{k_{max} - k_{min}}\right) \tag{35}$$

The surface curvature map generated from the quantification of local surface index is in the interval [0-1] and can also be employed to match two 3D fingerprint surfaces. In this work, we generated surface curvature map from every reconstructed 3D fingerprints and also employed them to ascertain possible performance improvement for the 3D fingerprint identification.

# 6. EXPERIMENTS AND RESULTS

In the best of our knowledge, there is no publicly available database for the 3D fingerprint images. Therefore we acquired 3D fingerprint database, using the approach

shown in Figure 1, from 240 distinct clients (by 'client', here, we refer a distinct finger, even if it belongs to the same person). We firstly acquired six images (impressions) from each of the fingers/clients which resulted in a total of 1440 impressions or 1440 3D fingerprint images reconstructed from 10080 2D fingerprint images. The imaging hardware was developed to generate illuminations from seven different LEDs while acquiring the 2D image from the corresponding illumination for each of the fingerprint impressions. The database was acquired during February 2012 to May 2012 in our university and is publicly available [43] to further research effort in this area. Each of the acquired 2D fingerprint images are downsampled by four and then used to automatically extract 500 × 350 pixels size (figure 7b-d) region of interest. This is achieved by subjecting the acquired images to an (Canny) edge detector and then scanning the resulting image from boundaries to locate image center which is used to crop fixed size region of interest images. There are several 2D minutiae matching algorithms available in the literature [21]-[24] and in this work we used BO-ZORTH3 [24] implementation from NIST which is available in public domain. Six 3D fingerprint images reconstructed from each of the 240 clients generated 3600 (240 × 15) genuine and 2064960 (240 × 6 × 239 × 6) impostor matching scores. The average number of 3D minutiae recovered from the 3D fingerprint images was 34.64 while the average number of 2D minutiae per 2D fingerprint image, acquired for the 3D fingerprint reconstruction, was 40.28.

**Figure 7:** (a) typical image sample from the 2D fingerprint image of
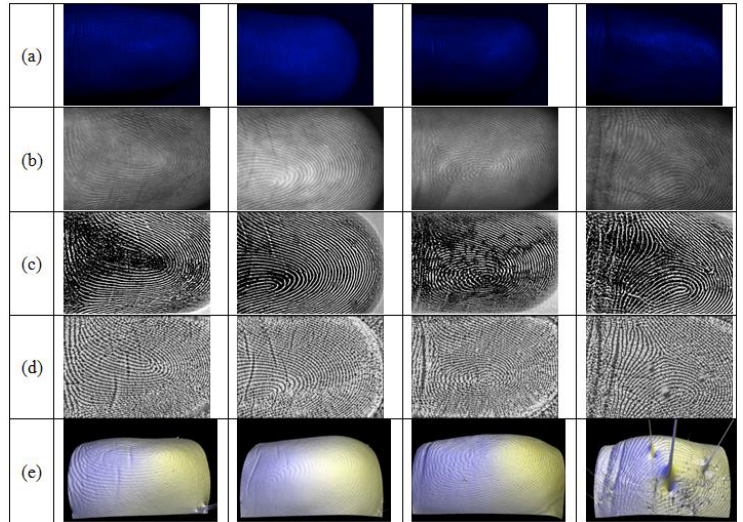


different clients, (b) image after image normalization, (c) corresponding enhanced images, (d) respective 3D surface curvature image and (d) reconstructed 3D fingerprint images.

Figure 7 illustrates 2D fingerprint image samples acquired from different clients and corresponding intermediate results during the preprocessing and 3D fingerprint reconstruction. Figure 8 shows image samples from the reconstructed 3D fingerprints using different least square solutions, *i.e.*, using Frankot and Chellappa algorithm [7] in figure 8 a-b and using Poisson solver [19] [29] in figure 8-c. It was observed that the use of normal amplification

filter increases the visibility of ridges but it introduces spurious points (random rapid change of height) on the reconstructed surface. The exclusion of this filter can help to eliminate such noisy high value odd point (figure 8-b). Poisson solver [19] generates direct analytical results to the least square problem by solving a Poisson equation has shown to generate 3D fingerprint surface which has close resemblances to its natural shape (figure 8-c). Our experiments for matching reconstructed 3D fingerprint minutiae achieved superior performance (figure 6 in conference version [39] of this paper) using this approach and this method was therefore preferred for further experimental results reported in this paper.
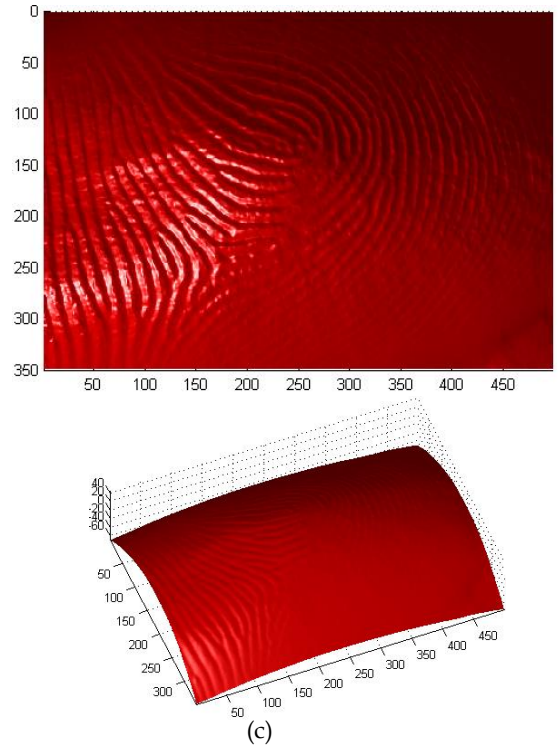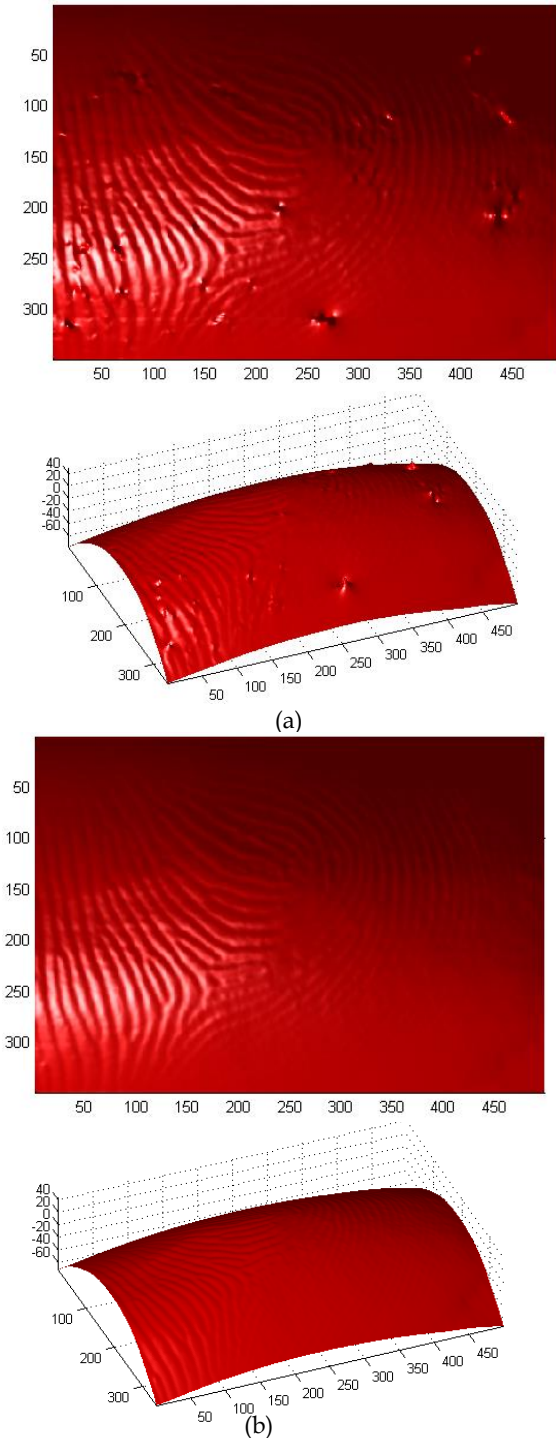


(a)



(b)



(c)

**Figure 8**: The 3D fingerprint surfaces are reconstructed (a) with normal amplification filter, (b) without normal amplification filter, and (c) without amplification filter using Poisson solver. The top views are in first row while the front views are on bottom row.

We firstly present the experimental results from the matching of 240 client's fingers from the authentication experiments. Multiple 2D fingerprint images acquired for
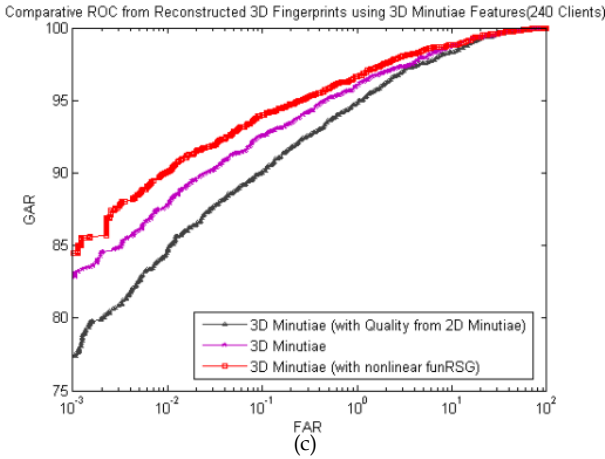


(a)



(b)

(c)
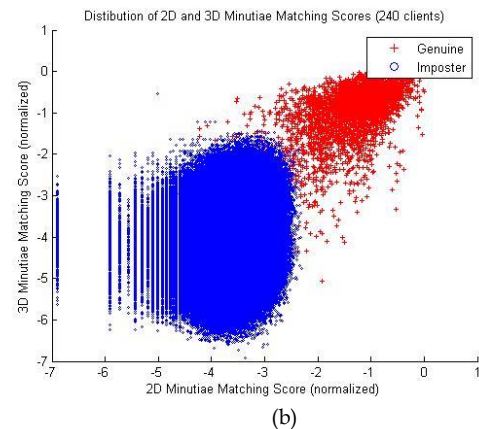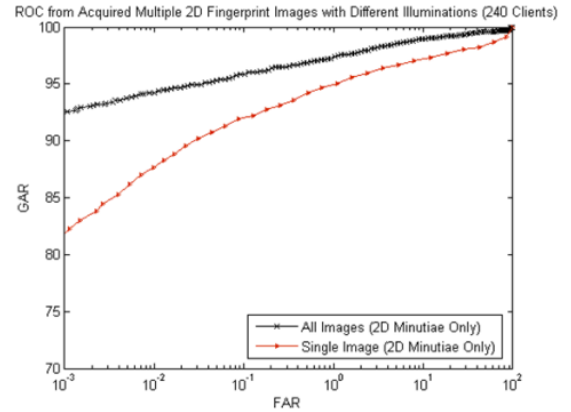
**Figure 9**: (a) The ROC using 2D fingerprint images with different illumination (240 clients), (b) distribution of 3D and 2D minutiae matching scores, (c) comparative performance from 3D minutiae matching strategies considered in experiments.
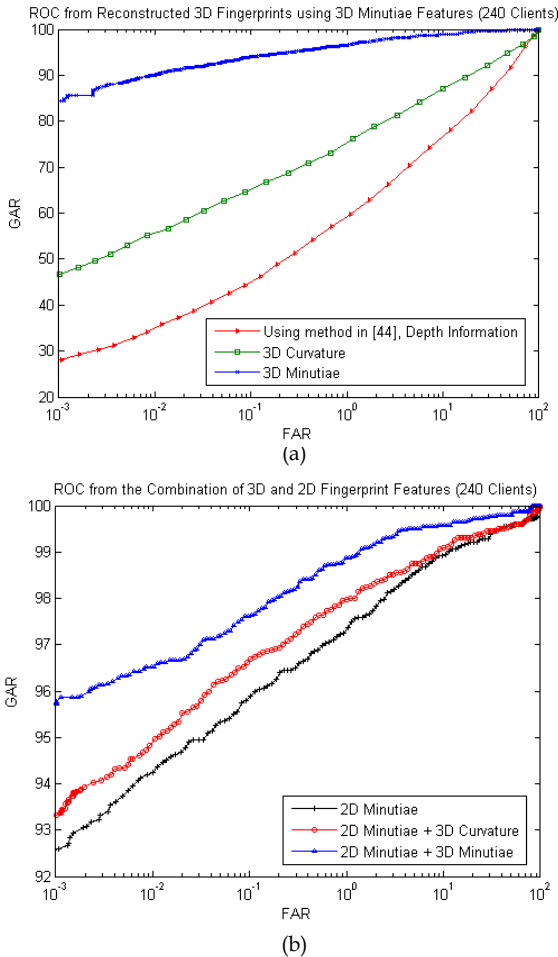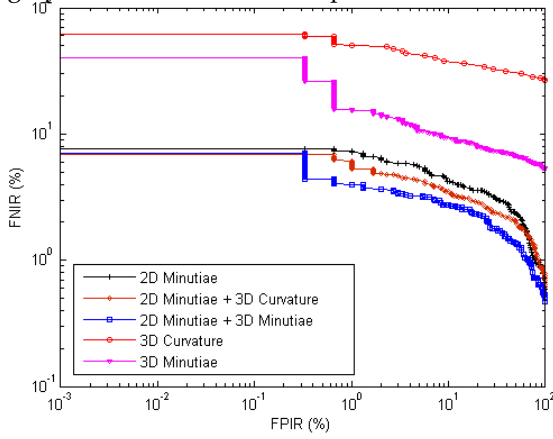

(a)


(b)

**Figure 10**: The receiver operating characteristics for the (a) relative/comparative performance using reconstructed 3D fingerprint images, and (b) performance using combination of 3D fingerprint and 2D fingerprint images acquired during photometric stereo based reconstruction.

the 3D fingerprint reconstruction can themselves be utilized for generating matching scores from the 2D fingerprintminutiae. However the nature of imaging employed requires that each of these 2D fingerprint images be acquired under different illumination as the 3D *shape from*
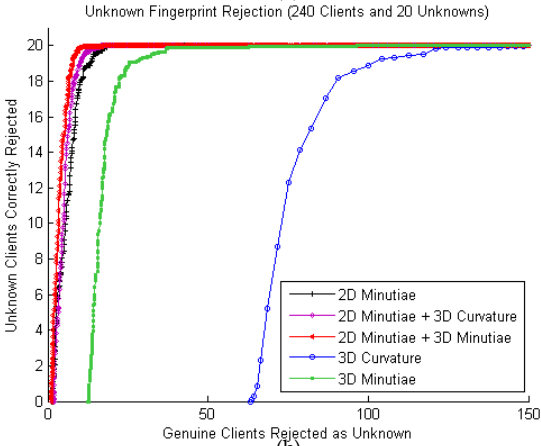
*shading* is the key to reconstruct 3D fingerprint information. Therefore the minutiae features extracted from the respective 2D fingerprint images can be different and we attempted to generate best matching scores by matching all the available 2D fingerprint images from two client fingers. Figure 9 illustrates experimental results from the usage of 2D fingerprint images when all such seven images corresponding to the query 3D fingerprint are matched with all the possible matches of the seven images from the corresponding *probe* 3D fingerprint and using the best matching score as the decision score (for genuine or impostor classification) from the 2D fingerprint matching. As shown in the receiver operating characteristics (ROC) from the experimental results in figure 9-a, such an approach generates superior performance as compared to the case when only the best performing 2D fingerprint matching score is employed as the decision score. Therefore in our further experiments, we employed this superior approach to generating 2D fingerprint matching scores, corresponding to the reconstructed 3D fingerprint, by using all respective 2D fingerprint images utilized for the 3D fingerprint reconstruction. Figure 9-b illustrates the distribution of (normalized) genuine and impostor matching scores obtained from 3D fingerprint and the corresponding 2D fingerprint matching. Figure 9-c illustrates the ROC generated from 3D fingerprint matching scores using two matching schemes discussed in section 4.3. These results suggest that the unified score based matching approach achieves superior performance and is therefore employed in our further experiments. We also employed the 2D minutiae quality [24], corresponding to the matched 3D minutiae during score generation in (20) and attempted to achieve performance improvement. However, as can also be seen from the results in figure 9-b, such an approach was not successful. This can be possibly attributed to the fact that 2D minutiae quality may be a reliable indicator for 3D minutiae quality and an independent indicator needs to be developed for 3D minutiae quality in the further extension of this work.

The ROC from matching 240 clients' images is shown in figure 10. This figure illustrates matching results using 3D minutiae representation and 3D fingerprint curvature representation. We also implemented 3D fingerprint matching approach described in [44] using the depth information. The ROC using this approach is also shown in figure 10-a for comparison. As can be observedfrom this ROC, the resulting performance (EER of 18.56%) is quite poor. Our database of 3D fingerprints (or 3D model of reconstructing the 3D information) illustrates *larger distortion* after flatting the images than those (flattening in reference [44]) from the structured lighting approach]. Significant degradation in performance (figure 10-a) from the depth information matching can be attributed to such distortion in the flatting of the 3D fingerprint model. Our 3D fingerprint model does not reconstruct fingerprints as cylinder-like (because our reconstructed area/volume sometimes is partial or not cylinder-like), therefore the observed distortion is larger since the model in [44] assumes that the 3D fingerprints can be segmented into slices like from the cylindrical portions. The difference in

the heights of the ridge and valley is also observed to be smaller on the edges of the reconstructed 3D fingerprints since our imaging setup uses the camera at the top/vertex (also such part of the valley is often occluded by ridges on the edges of 3D fingerprints). Our earlier efforts also investigated to reconstruct 3D fingerprints using non-Lambertian reconstruction model and results were not encouraging. The experimental results in figure 10-a suggest that the that 3D minutiae representation and matching approach developed in this work (section 4.2-4.4) achieves superior results as compared to those using 3D fingerprint surface curvature representation.
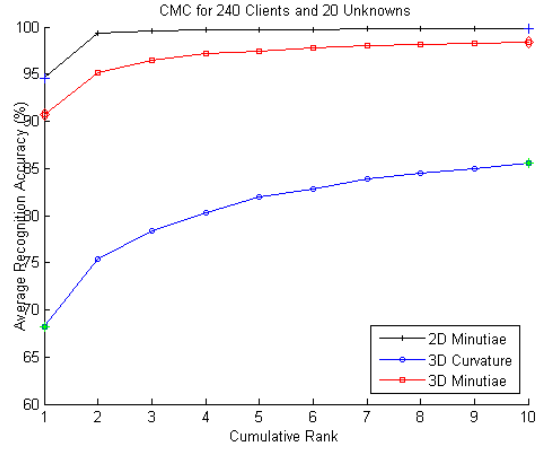
surface curvature representation, and 3D minutiae representation. This figure also illustrates matching results from corresponding 2D fingerprint images (reproduced from figure 9-a) employed during the 3D fingerprint reconstruction. The score-level combination[4] of matching scores using *adaptive fusion* [13] is employed in these experiments as it is judicious to exploit 3D matching scores only when the matching scores from 2D fingerprints are below some predetermined threshold. The threshold limit (figure 10-b) for 3D minutiae was empirically fixed to 0.1 while this limit while combining 3D surface curvature
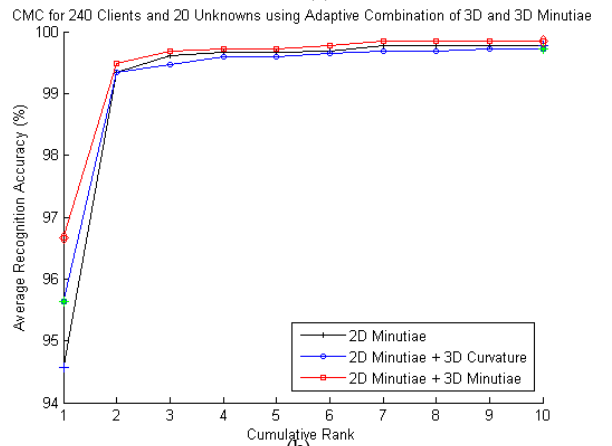


(a)



(b)

**Figure 11**: (a) FPIR Vs FNIR characteristics from the experiments and (b) corresponding performance for the unknown subject rejection using 240 clients and 20 unknowns.



(a)



(b)

**Figure 12**: The cumulative match characteristics for the (a) average recognition performance on using reconstructed 3D fingerprint images and (b) respective performance using combination of 3D and 2D fingerprint images.

was fixed to 0.09. It can be ascertained from this figure and the EER illustrated in Table 2 that the combination of 3D minutiae matching scores with the available 2D minu-

Figure 10-b illustrates experimental results from the combination of fingerprint matching scores using 2D minutiae representation (using the images acquired/available during 3D fingerprint reconstruction),

**Table 2**: Individual and Combined Match Performance from 2D and 3D Fingerprint Images.

| Experiments | 2D Minutiae | 3D Curvature | 3D Minutia | 2D Minutiae + 3D Curvature | 2D Minutiae + 3D Minutiae |
|---|---|---|---|---|---|
| *Equal Error Rate* from 240 clients (ROC in figure 10) | 2.12% | 12.19% | 2.73% | 1.73% | 1.02% |
| *Equal Error Rate* from 240 clients and 20 unknowns (DET in figure 11) | 5.44% | 32.26% | 9.28% | 4.36% | 3.33% |
| *Rank-1 accuracy* from 240 clients and 20 unknowns (CMC in figure 12) | 94.56% | 68.21% | 90.72% | 95.64% | 96.67% |

[4] Performance from other popular fusion approaches is also quite close and can also significantly improve the performance (more results in *supplementary* file).

tiae matching scores achieves superior performance. This performance improvement is significant and suggests that the 2D fingerprint images utilized for reconstructing 3D fingerprints, using photometric stereo, can be simultaneously used to improve the performance for the 3D fingerprint matchingAny automated biometric system is also expected to effectively identify the unknown clients, *i.e.*, able to reject those clients which are not enrolled in the database. In order to explicitly ascertain such capability, we additionally acquired 20 new clients' 3D fingerprint images and employed them as unknown clients. These unknown clients were then identified from the proposed approach to ascertain the performance. Figure 11-b shows the plot of number of unknown clients identified as unknown verses known clients rejected as unknown. These experimental results also suggest superior performance for the 3D minutiae representation and achieve further improvement with the combination of conventional 2D minutiae features. The performance from the proposed identification schemes for the FPIR (false positive identification rate) and FNIR (false negative identification rate) was also observed and is illustrated in figure 11-a.  The performance improvement using the combination of 3D minutiae representation, extracted from the reconstructed 3D fingerprint images, and 2D minutiae representation is observed to be quite consistent in FPIR Vs FNIR plots.

Although the key objective of our work was to develop a contactless 3D fingerprint verification approach, we also performed the experiments for the recognition tasks using the same protocol/parameters as used for figure 11 for the verification task. Figure 12 illustrates cumulative match characteristics (CMC) from the recognition experiments for the comparison and combination of 2D/3D fingerprint features. It is widely believed [30] that the verification and recognition are two different problems. However the illustrated results for recognition also suggest superior performance using 3D minutiae representation, over 3D curvature representation, and also illustrate improvement in average (rank-one) recognition accuracy using combination of available minutiae features from the 2D fingerprint images acquired during the 3D fingerprint reconstruction.

**Table 3**: 3D and 2D Fingerprint Correspondence Probabilities.

| $M, m, n, q$ | P(Fingerprint Correspondence) | |
| --- | --- | --- |
| | **2D** [28] | **3D** |
| 104, 26, 26, 26 | 5.27e-40 | 5.51e-57 |
| 104, 26, 26, 12 | 3.87e-9 | 8.94e-17 |
| 176, 36, 36, 36 | 5.47e-59 | 1.68e-82 |
| 176, 36, 36, 12 | 6.10e-8 | 1.90e-15 |
| 248, 46, 46, 46 | 1.33e-77 | 1.21e-107 |
| 248, 46, 46, 12 | 5.86e-7 | 2.46e-14 |
| 70, 12, 12, 12 | 1.22e-20 | 1.77e-28 |

In order to ascertain uniqueness of 3D fingerprints, we can compute the probability (20) that two arbitrary 3D minutiae from two different fingerprints can match with each other. Table 3 illustrates the probability of false random correspondence for matching two 3D minutiae, which uses same individuality model parameters empirically estimated for a 500 dpi sensor in [28], *i.e.*, $l = 0.267$,

with $k = 0.222$ which is estimated from our experiments for matching two 3D minutiae (the threshold limits of $\Delta r, \Delta_{A_\theta}, \Delta_{A_\phi}$ were 18, 20°, and 20° respectively).  The new/right column in table 3 illustrates the possible improvement in the uniqueness of fingerprints when the same minutiae features are matched in 3D space.

## 7.  SUMMARY AND FURTHER WORK

The minutiae features are widely considered to be most reliable and employed in most of the commercial and forensic fingerprint systems available today. This paper has proposed to further strengthen their distinctiveness by incorporating minutiae height $z$ and their 3D orientation $\phi$, with promising experimental results, to help in advancing the state-of-the-art in fingerprint matching techniques available today.  The use of 3D minutiae matching model developed in this paper also reveals the extent of possible improvement in the currently believed theoretical estimates on the individuality of fingerprint as biometric modality. Our efforts in this work have been inspired by the need to develop alternative methods to address a key limitation of existing 3D fingerprint technologies which require structured lighting, or multiple cameras. In addition to providing significantly improved performance than what can be possible using contactless 2D fingerprints, single camera-based 3D fingerprint identification can significantly reduce the bulk and the cost associated with the structured lighting or multiple camera based currently introduced 3D fingerprint identification methods. Our efforts to develop a robust 3D fingerprint feature extraction algorithm and an effective matching strategy for combining multiple pieces of information, generated during the 3D fingerprint reconstruction and feature extraction process, have yielded promising insights and results. The experimental results presented in this paper suggest the usefulness of this approach by illustrating higher accuracy and reliability than those using currently employed/deployed contactless 2D fingerprint technologies while requiring only single camera to automatically extract 3D fingerprint features. The (first) public availability of 1560 3D fingerprint database generated from this study, using 260 clients (all images) will help to further research efforts in this area.

One of the most fundamental questions one would like to ask about any biometrics system is [28]; what is the inherent discriminable information which can be recovered from the input signal? The model considered to ascertain 3D individuality is inherently simple and does not consider dependencies among features. However, a first-order approximation to answer such fundamental question will have a significant bearing on the acceptance of emerging 3D fingerprint technologies.

Despite promising results and success in developing low-cost 3D fingerprint solution, one paper cannot address several open issues and these can be summarized in the following for further work. The performance from 3D fingerprint minutiae matching is lower than those achieved from the 2D minutiae in our experiments. There can be two plausible explanations for such discrepancy.

Firstly, all the seven 2D fingerprint images are employed to generate 2D minutiae matching scores while only one reconstructed 3D fingerprint is used for generating 3D minutiae matching performance. Secondly, the reconstruction error in the 3D fingerprint surface reconstruction can degrade 3D minutiae matching performance. When the reconstructed surface is not consistent, the difference in depth value $z$ and angle $\phi$ is expected to increase the distance between the 3D minutiae from the genuine matches resulting in performance degradation. Therefore further improvement in the reconstruction accuracy is expected to improve performance from 3D minutiae matching. In this context, surface reconstruction using a continuum of solvers, *e. g.* regularization, m-estimators, diffusion, as attempted in [19], can be explored in the further work to ascertain higher accuracy in the 3D fingerprint surface reconstruction. The matching matric explored in (22) needs to be further evaluated, especially to ascertain $f(r)$ which was fixed (21) in our experiments. The 3D fingerprint individuality model developed in section 4.5 does not account for errors in the localization and detection of 3D minutiae. Therefore this model requires improvement to account for uncertainty in recovering (true) 3D minutiae while considering some kind of interdependence between features. The quality of 3D reconstruction algorithm can impact the matching accuracy of 3D fingerprints which requires in depth study in the further extension of this work. In addition, further work is also required to ascertain 3D fingerprint deformations due to external pressure, wrinkles [46], and incorporate such deformation models [47] for more accurate matching. The 3D fingerprint database made available from this work to the researchers and developers should help to promote further research efforts in this area. *Although much more work remains to be done, the experimental results and generalized 3D minutiae matching model presented in this paper indicate that the contactless 3D fingerprint identification can constitute a promising addition to state-of-the-art in biometrics security.*

## REFERENCES

[1] G. Parziale and Y. Chen, "Advanced technologies for touchless fingerprint recognition," *Handbook of Remote Biometrics*, M. Tistarelli, Stan. Z. Li, R. Challeppa, (*Eds*.), pp. 83-109, Springer-Verlag London, 2009.

[2] *Shape from Shading*, B. K. P. Horn and M. J. Brooks (*Eds*.), MIT Press, Cambridge, MA, 1989.

[3] Y. Wang, Q. Hao, A. Fatehpuria, D. L. Lau and L. G. Hassebrook, "Data acquisition and quality analysis of 3-Dimensional fingerprints," *Proc. IEEE conference on Biometrics, Identity and Security*, Tampa, Florida, Sep. 22-24, 2009.

[4] Y. Wang, D. L. Lau and L. G. Hassebrook, "Fit-sphere unwrapping and performance analysis of 3D fingerprints," *Applied Optics*, vol. 49, no. 4, pp. 592-600, 2010.

[5] *Handbook of Fingerprint Recognition*, D. Maltoni, D. Maio, A. K. Jain, and S. Prabhakar, Springer Verlag, Second Ed., 2009.

[6] R. J. Woodham, "Gradient and curvature from photometric stereo including local confidence estimation," *J. Opt. Soc. America*, no. 11, pp. 3050-3068, 1994.

[7] R. T. Frankot and R. Chellappa, "A method for enforcing integrability in shape from shading algorithms," *IEEE Trans. Pattern Anal. Mach. Intell.*, vol. 10, no. 4, pp. 439 - 451, Jul. 1988.

[8] G. Parziale, E. Diaz-Santana and R. Hauke, "The surround imager: A multi-camera touchless device to acquire 3d rolled-equivalent fingerprints," *Proc. ICB 2006*, LNCS, vol. 3832, 2006.

[9] A. Belyaev, "Mesh Smoothing and Enhancing. Curvature Estimation," Saarbrucken, 2006.
*www.mpi-inf.mpg.de/~ag4-gm/handouts/06gm_surf3.pdf*

[10] Goldfeather and V. Interrante, "A novel cubic-order algorithm for approximating principal direction vectors," *ACM Trans. Graphics*, vol. 23, no. 1, pp. 45-63, 2004.

[11] S. Yoshizawa, A. Belyaev, and H.-P. Seidel, "Fast and robust detection of crest lines on meshes," *Computer Aided Geometric Design* (CAGD), Vol. 25, Issue 8, pp. 545-560, 2008.

[12] C. Dorai and A. K. Jain, "COSMOS — A representation scheme for 3D free-form objects," *IEEE Trans. Patt. Anal. Mach. Intell.*, vol. 19, no. 10, pp. 1115-1130, 1997.

[13] V. Kanhangad, A. Kumar and D. Zhang, "A unified framework for contactless hand verification," *IEEE Trans. Info. Forensics & Security*, pp. 1014-1027, 2011.

[14] A. K. Jain and A. Kumar, "Biometrics of second generation: an overview," *Second Generation Biometrics*, E. Mordini, and T. Dimitros (*Eds*.), Springer 2012.

[15] L. Hong, Y. Wan and A. K. Jain, "Fingerprint image enhancement: algorithms and performance evaluation," *IEEE Trans. Patt. Anal. Mach. Intell.*, vol. 20, pp. 777-789, Aug. 1998.

[16] J.-F. Lalonde, N. Vandapel and M. Hebert, "Automatic three-dimensional point cloud processing for forest inventory," *Technical Report No. MU-RI-TR-06-21*, Robotics Institute, Pittsburgh, PA, 2006.

[17] N. A. Vandal and M. Savvides, "CUDA accelerated iris template matching on graphics processing," *Proc. BTAS 2010*, pp. 1-7, 27-29, Sept 2010.

[18] A. Kumar and Y. Zhou, "Human identification using finger imaging," *IEEE Trans. Image Process.*, vol. 21, pp. 2228-2244, April 2012

[19] A. Agrawal, R. Raskar and R. Chellappa, "What is the range of surface reconstructions from a gradient field?," *Proc. 9th European Conference on Computer Vision*, Graz, Austria, May 2006. http://mesh.brown.edu/taubin/pdfs/taubin-eg00star.pdf

[20] G. Taubin, "Geometric signal processing on polygonal meshes," *Eurographics State of the Art Reports*, 2000.

[21] A. K. Jain, L. Hong and R. Bolle, "On-line fingerprint verification, *IEEE Trans. Pattern Anal. Mach. Intell.*, vol. 19, no. 4, pp. 302-314, 1997.

[22] M. Tico and P. Kuosmanen, "Fingerprint matching using an orientation-based minutiae descriptor," *IEEE Trans. Pattern Anal. Mach. Intell.*, vol. 28, no. 8, pp. 1009-1014, Aug. 2003.

[23] B. V. K. Vijay Kumar, M. Savvides, C. Xie, K. Venkataramani, J. Thorton, and A. Mahalanobis, "Biometric verification with correlation filters," *Appl. Optics*, vol. 43, 391-402, 2004.

[24] NIST Biometric Image Software, NBIS Release 4.1.0, http://www.nist.gov/itl/iad/ig/nbis.cfm, 2011.

[25] http://en.wikipedia.org/wiki/Atan2, accessed Jan. 2012.

[26] B. Bringier, A. Bony and M. Khoudeir, "Specularity and shadow detection for the multisource photometric reconstruction of a textured surface," *J. Opt. Soc. Am. A., Opt Image Sci. Vis.*, vol. 29, pp. 11-21, Jan. 2012.

[27] M. Kucken and A. C. Newell, "Fingerprint formation,", *J. Th.*

*Biology*, vol. 235, pp. 73-81, 2005.

[28] S. Pankanti, S. Prabhakar, and A. K. Jain, "On the individuality of fingerprints," *IEEE Trans. Pattern Anal. Mach. Intell.*, vol. 24, pp. 1010-1025, Aug. 2002.

[29] T. Simchony, R. Chellappa, and M. Shao, "Direct analyatical methods for solving poisson equations in computer vision problems," *IEEE Trans. Pattern Anal. Mach. Intell.*, pp. 435-436, Dec. 1990.

[30] R. M. Bolle, J. H. Connell, S. Pankanti, N. K. Ratha, A. W. Senior, "The relation between ROC and the CMC," *Proc. AutoID 2005*, pp. 15-20, 2005.

[31] Flashscan3d, http://www.flashscan3d.com, accessed Aug. 2012

[32] T.-Y. Jea and V. Govindaraju, "A minutiae-based partial fingerprint recognition system," *Pattern Recognition*, vol. 38, no. 10, pp. 1672-1684, 2005.

[33] Y. Chen, G. Parziale, E. Diaz-Santana, and A. K. Jain, "3D Touchless fingerprints: Compatibility with legacy rolled images," *Proc. BCC 2006*, Tampa, 2006.

[34] J. Feng, "Combining minutiae descriptors for fingerprint matching," *Pattern Recognition*, vol. 41, no. 1, pp. 342-352, 2008.

[35] TBS, http://www.tbs-biometrics.com, Accessed August 2012

[36] Y. Wang and J. Hu, "Golden ridge orientation modeling for partial fingerprint identification," *IEEE Trans. Patt. Anal. Mach. Intell.*, vol. 33, pp. 72-87, Jan. 2011.

[37] S. Shafaei, T. Innac, L. G. Hassebrook, "A new approach to unwrap a 3-D fingerprint to a 2-D Rolled equivalent fingerprint," *Proc. BTAS 2009*, Washington DC, Sep. 2009.

[38] A. Kumar and Y. Zhou, "Contactless fingerprint identification using level zero features," *Proc. CVPR 2011*, pp. 114-119, CVPRW'11,Colarado Springs,  June 2011.

[39] A. Kumar and C. Kwong, "Towards Contactless, Low-Cost and Accurate 3D Fingerprint Identification," *Proc. CVPR 2013*, pp. 3438-3443, Portland, Oregon, June 2013.

[40] H. Choi, K. Choi and J. Kim, "Mosaicing touchless and mirror-reflected fingerprint images," *IEEE Trans. Info. Forensics & Security*, no. 5, pp. 52-61, Mar. 2010.

[41] F. Chen, "3D fingerprint and palm print data model and capture devices using multi structured lights and cameras," *US Patent No. 7609865*, Oct. 2009.

[42] G. Paar, M. d. P. C. Perucha, Arnold Bauer, B. Nauschnegg, "Photogrammetric fingerprint unwrapping," *J. Appl. Geodesy*, vol. 2, pp. 13-20, 2008.

[43] The Hong Kong Polytechnic University 3D Fingerprint Images Database, 2012.
http://www.comp.polyu.edu.hk/~csajaykr/3Dfingerprint.htm

[44] Y. Wang, L. G. Hassebrook, D. L. Lau, "Data acquisition and processing of 3-D fingerprints," *IEEE Trans. Info. Forensics & Security*, pp, 750-760, Dec. 2010.

[45] L. Liu, T. Jiang, J. Yang, and C. Zhu, "Fingerprint registration by maximization of mutual information," *IEEE Trans. Image Process.*, vol. 15, no. 5, pp. 1100-1110, May 2006

[46] P. Krishnasamy, S. Belongie, D. Kriegman, "Wet fingerprint recognition: challenges and opportunities," *Proc. IJCB 2011*, pp. 1-7, Washington DC, Sep. 2011.

[47] K. Dandekar and M. A. Srinivasan, "Role of mechanics in tactile sensing of shape," *Touch Lab Report 2*, RLE TR-604, MIT, Cambridge, 1997.

[48] S. C. Dass, "Assessing fingerprint individuality in presence of noisy minutiae," *IEEE Trans. Info. Forensics & Security*, vol. 5, no. 1, pp. 62-70, Mar. 2010.

# Appendix A

## Probability of False Random Correspondence using 3D Minutiae Matching

Let $P$ and $Q$ denote two typical 3D minutiae templates, with $m$ and $n$ number of recovered true minutiae respectively, available for the matching.

$$P = \{(x_1, y_1, z_1, \theta_1, \phi_1), \dots, (x_m, y_m, z_m, \theta_m, \phi_m)\} \quad (A1)$$
$$Q = \{(x'_1, y'_1, z'_1, \theta'_1, \phi'_1), \dots, (x'_n, y'_n, z'_n, \theta'_n, \phi'_n)\} \quad (A2)$$

After alignment, minutiae $i$ in the template $Q$ is matched to minutiae $j$ in template $P$ if and only if,

$$\sqrt{(x'_i - x_j)^2 + (y'_i - y_j)^2 + (z'_i - z_j)^2} \leq r_0 \quad (A3)$$
$$\min(|\theta'_i - \theta_j|, 360 - |\theta'_i - \theta_j|) \leq \theta_0 \quad (A4)$$
$$\min(|\phi'_i - \phi_j|) \leq \phi_0 \quad (A5)$$

where $r_0$, $\theta_0$ and $\phi_0$ are the tolerance in distance and tolerance in angles respectively. Let $V$ be the overlapping volume between two arbitrary 3D fingerprint surface being matched while $H(p)$ be the height of the aligned surface with point $p$ on the projection on X-Y plane. $V$ can be estimated as follows:

$$U = \sum_{s=1}^{N} \sum_{t=1, t \neq s}^{N} \frac{\sum_{p \in A} |H(p)_s - H(p)_t|}{A(s,t)} \quad (A6)$$
$$\sigma = \sum_{s=1}^{N} \sum_{t=1, t \neq s}^{N} \frac{(\sum_{p \in A}(|H(p)_s - H(p)_t| - U)^2)}{A(s,t)} \quad (A7)$$
$$V = (U + 2\sqrt{\sigma})A(s,t) \quad (A8)$$

where $A(s, t)$ is the overlapped area on X-Y plane of two aligned surfaces $s$ and $t$. The variance $\sigma$ can be estimated by statistics of the reconstructed 3D fingerprint surface in the database and represents twice standard deviation limits that cover 95% confidence interval. The probability of a 3D minutiae in a template matched with an arbitrary minutiae is given by:

$$P\left(\sqrt{(x'_i - x_j)^2 + (y'_i - y_j)^2 + (z'_i - z_j)^2} \leq r_0\right) = \frac{\text{volume of tolerance}}{\text{volume of overlap}} = \frac{\frac{4}{3}\pi r_0^3}{V} = \frac{C}{V} (A9)$$
$$P(\min(|\theta'_i - \theta_j|, 360 - |\theta'_i - \theta_j|) \leq \theta_0) = \frac{\text{angle of tolerance}}{\text{total angle}} = \frac{2\theta_0}{360} (A10)$$
$$P(\min(|\phi'_i - \phi_j|) \leq \phi_0) = \frac{\text{angle of tolerance}}{\text{total angle}} = \frac{2\phi_0}{180} \quad (A11)$$

Assuming $(x, y, z)$ and $(x', y', z')$ are independent in (9), $\theta$ and $\theta'$ are independent in (10), and $\phi$ and $\phi'$ are independent. Let $J = \frac{V}{C}$, and assuming $J$ is the nearest integer. We can use similar formulation as in [28] to compute the probability, when there can be exactly $p$ matched minutiae among $n$ minutiae in template $Q$ and $m$ minutiae in template $P$ as follows:

$$P_{3D}(J, m, n, p) = \frac{\binom{m}{p}\binom{J-m}{n-p}}{\binom{J}{n}} \quad (A12)$$

When $p$ minutiae's positions being matched as in above equation, the probability of $q$ minutiae's direction $\theta$ being matched can be estimated as follows:

$$\binom{p}{q}(l)^q(1 - l)^{p-q} \quad (A13)$$

where $l$ is same as computed in equation (10). The probability of matching $q$ minutiae in both position $(x, y, z)$ and direction $\theta$ can be written as follows:

$$P_{3D}(J, m, n, q) = \sum_{p=q}^{\min(m,n)} \left( \frac{\binom{m}{p}\binom{J-m}{n-p}}{\binom{J}{n}} \times \binom{p}{q}(l)^q(1 - l)^{p-q} \right)(A14)$$

With $q$ minutiae's position and direction $\theta$ already being matched, the probability of $r$ minutiae's direction $\phi$ being matched can be estimated as follows:

$$\binom{q}{r}(k)^r(1 - k)^{q-r} \quad (A15)$$

where $k$ is same as estimated using equation (A11). The probability of matching $r$ minutiae in two 3D fingerprint templates in both position $(x, y, z)$ and spatial-orientation $\theta$ and $\phi$, can be written as follows:

$$P_{3D}(J, m, n, r) = \sum_{p=r}^{\min(m,n)} \sum_{q=r}^{p} \left( \frac{\binom{m}{p}\binom{J-m}{n-p}}{\binom{J}{n}} \times \binom{p}{q}(l)^q(1 - l)^{p-q} \times \binom{q}{r}(k)^r(1 - k)^{q-r} \right)(A16)$$

The probability of false random correspondence using conventional minutiae representation in 2D space i.e., matching $q$ minutiae both in spatial-location $(x, y)$ and also along the direction $\theta$, is given by:

$$P_{2D}(M, m, n, q) = \sum_{p=q}^{\min(m,n)} \left( \frac{\binom{m}{p}\binom{M-m}{n-p}}{\binom{M}{n}} \times \binom{p}{q}(l)^q(1 - l)^{p-q} \right) \quad (A17)$$

where $M$ represents the nearest integer for $M = A/(\pi r_0^2)$. Assuming that the *same* two fingerprints are matched in 2D space and 3D space, and $J = M$, using (A17) we can rewrite (A16) as in the following.

$$P_{3D}(M, m, n, r) = \sum_{q=r}^{p} \left( \binom{q}{r}(k)^r(1 - k)^{q-r} \right) \times P_{2D}(M, m, n, q) \quad (A18)$$